J Mater Sci: Mater Electron (2018) 29:467–473
DOI 10.1007/s10854-017-7935-x

Investigation of sensing properties of sol–gel processed 4 at%Sb:SnO_2/TiO_2 thin films

Miguel H. Boratto[1,2] · Roberto A. Ramos Jr.[1] · Luis V. A. Scalvi[1,2]

Received: 31 August 2017 / Accepted: 28 September 2017 / Published online: 10 October 2017

Abstract In this work we investigate the gas and photo sensing properties of the antimony doped tin oxide and titanium oxide (4 at%Sb:SnO_2/TiO_2) nanocrystalline thin films deposited by sol–gel dip-coating. Photoconductivity measurements are carried out under solar light spectra irradiation at different powers. These results show a photo sensitivity of the films in a lateral junction due to interfacial defects. Gas sensitivity was studied at different pressures, and higher conductivity is presented at lower pressure compared to oxygen-rich atmosphere. It occurs due to absence of oxygen adsorption on the semiconductors surface. TiO_2 films are also investigated concerning its properties to gas sensing under photo-excitation with InGaN LED light source with wavelength centered in 450 nm. The decay of photo-induced current evaluated under O_2 and vacuum atmospheres shows that the sample illumination may contribute to higher gas-sensitivity. This measurement allows determining the charge carrier capture energy, that is related to trapping dominated by distinct defects in each atmosphere.

1 Introduction

Titanium dioxide (TiO_2) is an oxide semiconductor material that presents wide bandgap, about 3.3 eV. High interest in controlling the TiO_2 structure is due to the direct dependence of its properties with structure [1]. For instance, gas sensor application with TiO_2 is improved with preferential growth of the anatase structure on (101) and (001) (hkl) plans [2, 3]. The presence of oxygen vacancies in this oxide facilitates the gas adsorption on surface, which makes stronger bonding between the gas molecules and the film surface [3]. The response time to gas sensing of this material is short, i.e. for TiO_2 particles size in the range of 3–50 nm, the response time is < 1 min at high temperature.

Tin dioxide (SnO_2) is also a wide bandgap oxide semiconductor (3.6–4 eV) that presents high transparency in the visible region, low resistivity and high thermal stability [4, 5]. When n-doped with Sb^{5+}, the SnO_2 presents higher conductivity through a higher concentration of free electrons [6], but with high resistance due to grain boundary scattering that decreases considerably the electron mobility [6, 7]. Complex TeraHertz transmission performed in pellets of nanoparticles with different levels of doping and thermal annealing indicates the presence of energy barriers suppressing the charge transport between nanoparticles [8].

A junction formed by two different n-type semiconductor may present rectifier characteristics if a barrier is developed between the conduction bands due to their different electron affinity [9]. Depletion regions may exist on both sides of the interface, but the possible presence of interface states which accept electrons may increase considerably the energy barrier [9]. Both TiO_2 and 4 at%Sb:SnO_2 materials investigated in this work present oxygen vacancies [10, 11] that can act as such interfacial states. The electron affinity is close for these materials (4.5 eV for SnO_2 [12] and 5.0 eV for TiO_2 [13]). Although it is slightly higher for TiO_2, the discontinuity of the conduction bands [14] leads to a small potential barrier of approximately 0.5 eV. The 4 at%Sb:SnO_2/TiO_2 junction may present gas sensing properties due to their oxygen vacancies [3] which are well known for applications as

✉ Miguel H. Boratto
miguel@fc.unesp.br

[1] POSMAT - Post-Graduate Program in Materials Science and Technology, School of Sciences, São Paulo State University (UNESP), Bauru, São Paulo 17033-360, Brazil

[2] Department of Physics, School of Sciences, São Paulo State University (UNESP), Bauru, São Paulo 17033-360, Brazil

sensor of O_2, CO_2 and CH_4 gases [15]. Besides the sensing properties, this junction, in quite different configurations, has been applied to memristors [12], optoelectronics [16], photocatalytic [17] and photovoltaic applications [18].

Both SnO_2 and TiO_2 have been reported to be obtained through expensive and/or high-vacuum methods such as magnetron sputtering [19], atomic layer deposition [20], laser chemical vapor deposition [21], spray pyrolysis deposition [22], among others. In this work we obtain both thin films by a relatively simple and low cost approach, the sol–gel method, that also presents advantages through film deposition on complex substrate surfaces. We investigate the electrical properties, and photo and gas sensitivity of the lateral junction architecture of 4 at%Sb:SnO_2/TiO_2 deposited by sol–gel dip-coating. We evaluate the influence of the metal/semiconductor and semiconductor/semiconductor interface on the charge transport, as well the defects presented on the semiconductors thin films. The TiO_2 thin film is also evaluated considering its gas sensing enhancement under monochromatic light excitation through measuring the decay of photo-induced current and theoretical analysis. Concerning the sample illumination, the device architecture (lateral junction) used in this work, has sensible contribution, due to optimized irradiation area. This potential enhancement may contribute to increasing the efficiency of gas sensing properties of the lateral junction Sb:SnO_2/TiO_2.

2 Experimental details

2.1 Thin films synthesis

Sol–gel fabrication of TiO_2 was carried out by hydrolysis and condensation of titanium (IV) isopropoxide using a high molar ratio of water:alkoxide (200:1), isopropanol as co-solvent, HNO_3 as catalyst, and Triton X-100 as surfactant [11, 23, 24]. Initially 2.6 ml of Nitric acid was added to 185 ml of deionized water and 57 ml of isopropanol solution, followed by dropwise addition of 15 ml of titanium (IV) isopropoxide alkoxide under stirring and heated at 85 °C for 4 h. The concentration of solution was performed by evaporating the solvent and dispersants at 100 °C until reach a volume of 50 ml, which was followed by the addition of the surfactant, under stirring for 30 min.

Colloidal suspension of 4 at%Sb:SnO_2 was obtained through an aqueous solution of Sn^{4+} (0.5 M) obtained by dissolution of $SnCl_4{\cdot}5H_2O$ in deionized water mixed to a solution of Sb obtained by dissolution of SbF_3 in deionized water. Hydrolysis of Sn^{4+} and Sb^{5+} ions were promoted by addition of NH_4OH. The suspension was submitted to dialysis against distilled water for elimination of chloride and fluoride ions [7, 25].

The deposition of sol–gel was carried out by dip coating, on soda lime substrate previously cleaned with piranha solution at H_2SO_4:H_2O_2 ratio of 70:30, with immersion/emersion speed of 10 cm/min and calcination of 80 °C for 10 min. A total repetition of 10 times for Sb:SnO_2 and 5 times for TiO_2 was done in order to obtain the semiconductors films. The final thermal annealing occurred at 500 °C for 2 h after individually deposition of both films for structural and optical characterization, as well as both films together in a lateral junction architecture as presented in Fig. 1a. Figure 1b shows a sample with only TiO_2 thin film deposited as previously described. After thermal annealing Al electrodes were deposited through thermal evaporation, with thickness of 100 nm, at pressure of about 10^{-6} torr, on top of the films to allow electrical characterization. The width (W) of Al contacts and length (L) between each one was W = 10 mm and L = 20 mm.

2.2 Characterization

X-ray Diffraction (XRD) was performed on Rigaku diffractometer (Model D/Max—2100/PC) operating with CuKα radiation (1.5405 Å) and Ni filter for Kβ radiation. The measurement range was from 20° to 80° with a scanning rate of 2°/min, in 2θ mode for films at fixed incident angle of 1.5°. Data were analyzed with the Match software (Crystal Impact). The average crystallite size was estimated by Scherrer Equation [7]. Transmittance and absorbance were performed in a Perkin Elmer spectrophotometer (Lambda Model 1050 UV/VIS/NIR) in the range of 200–3300 nm. Evaluation of the optical bandgap was performed by using Tauc method [26]. Photocurrent as function of voltage applied was performed in a Newport Power supply 69907, using a Xenon Lamp (150 W) with a filter AM 1.5 that corresponds the solar light emission, with maximum incident

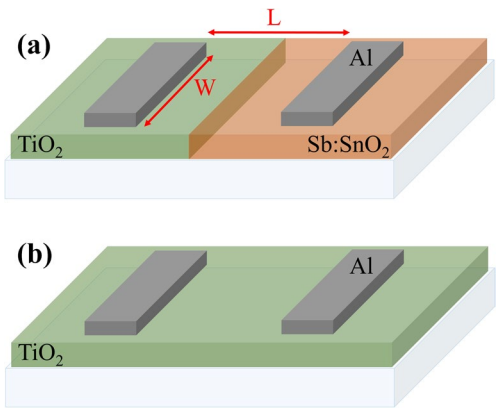

Fig. 1 Diagrams of the samples **a** with 4 at%Sb:SnO_2/TiO_2 semiconductor films deposited side-by-side and **b** only TiO_2 thin film deposited. Both samples present Al top electrodes for electrical characterization

power of about 96 mW/cm^2 on the sample. Photocurrent decay under vaccum and O_2 atmospheres was carried out at room temperature with photoexcitation source of InGaN LED (wavelength from 430 to 470 nm, centered in 450 nm) for 90 s at fixed applying voltage V = 2 V.

3 Results and discussions

3.1 Individual TiO_2 and SnO_2 layers

In order to understand the electrical transport processes within the devices with both 4 at%Sb:SnO_2 and TiO_2 thin films as active semiconducting layer, a structural and optical analysis was performed in both individual films. Figure 2a presents the transmittance (inset) and optical bandgap of the 4 at%Sb:SnO_2 thin film deposited on glass substrate. The bandgap was estimated through the Tauc method, and the value of the indirect bandgap is 3.6 eV, in good agreement with published results [7, 27]. Figure 2b shows the transmittance (inset) of the TiO_2 layer and its indirect bandgap estimative of 3.4 eV, also in agreement with published data [1, 11]. The thickness of both films were estimated through the interference fringes present in the transmittance data [28], and the values are 380 nm for Sb:SnO_2, and 360 nm for TiO_2 films.

XRD was carried out in order to investigate the structure and crystallite size of each semiconductor, with thermal annealing at 500 °C for 2 h. Fig. 3a shows the diffractogram of the 4 at%Sb:SnO_2 that presents rutile structure (JCPDS 088-0287) with most intense peak related to (101) plane. No presence of Sb in the crystalline lattice is noted in the diffractogram. The average crystallite sizes were calculated through Scherrer equation and found to be about 5 nm. The TiO_2 diffractogram is shown in Fig. 3b. The anatase structure is found in this material (JCPDS 089-4921) with

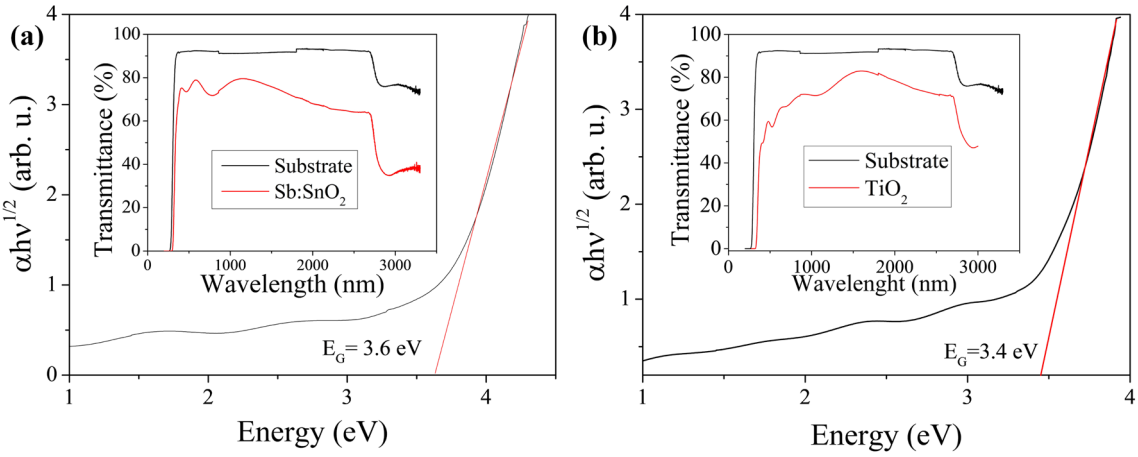

Fig. 2 Tauc plot and UV-Vis-NIR transmittance (*inset*) of the **a** 4at%Sb:SnO_2 and **b** TiO_2 thin films deposited on glass substrate

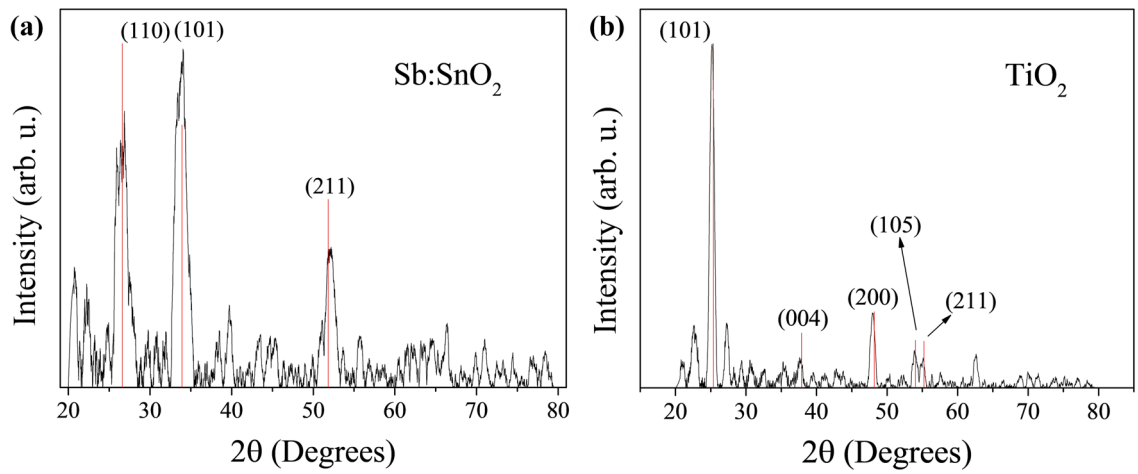

Fig. 3 Diffractograms of the **a** Sb:SnO_2 thin film on glass substrate with rutile structure, and **b** TiO_2 thin film with anatase structure

average crystallite size of about 10 nm. The small crystallite sizes obtained in both samples contribute strongly to the carrier scattering on the grain boundaries, which has high influence on the reduction of semiconductor conductivity [12, 25, 29]. When in lateral junction, the distinction on crystalline phases of SnO_2 and TiO_2 itself is not responsible for electrical transport properties of the device, due to the nanocrystalline nature of both films. The electrical conduction will be independent on each film, and the overall device properties must be determined by the semiconductors interface as well as the metal–semiconductor interfaces. The interface between semiconductors must be the region that presents the higher concentration of defects in the sample, mostly due to the junction of two highly disordered materials.

3.2 Electrical characterization of Sb:SnO_2/TiO_2 lateral junction

The 4at%Sb:SnO_2/TiO_2 in lateral junction architecture is investigated through photo and gas sensing characterizations in order to relate the sole properties of each film, as well as the influence of the multiple interfaces in the devices with the overall sensing properties obtained in this section. Figure 4 shows current *vs* voltage curves under solar light spectra photoexcitation at different powers under room atmosphere. The positive terminal is connected to the TiO_2 semiconductor. The result presents the photoconductivity of the lateral junction under different power light irradiating the samples. After photoexcitation with solar light, which presents a large spectrum of energy, the releasing of carrier from electron excitation and from different trap states increases the density of carrier in the material, which results on the higher current presented for higher power light. A high quantity of state-defects located at grain boundaries is present in the semiconductor layers due to oxygen vacancies present in both semiconductors [30, 31]. Such defects work as traps for charge carriers, and the photoexcitation with wide range spectra is responsible for releasing charge from wide range energies. As the photoexcitation of wide range wavelength was fixed and just the intensity was varied, it implies that the increase in electric current in these samples occurs only by increasing the number of free carriers released from similar energies.

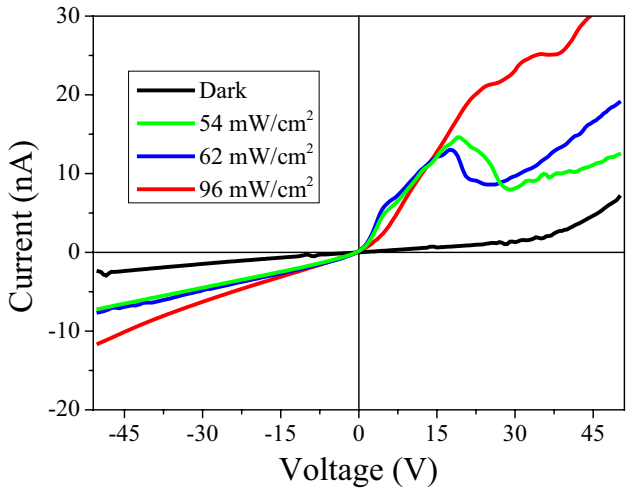

Fig. 4 Current vs Voltage of the 4at%Sb:SnO_2/TiO_2 lateral junction as function of the power of solar light spectra photoexcitation. Distance between contacts L = 10 mm

From Fig. 4 one can note that with photoexcitation, even for low power light, the current immediately increases at low positive voltages. Current taken at V = 40 V shows increase of about 878% after excitation at 96 mW/cm^2, compared to sample with no photoexcitation, whereas for powers of 62 and 54 mW/cm^2 electric current intensification of 466 and 351%, respectively, are obtained. It is worth noting the rectifying behavior presented at negative bias region, which yields mostly of the current through charge carriers releasing at positive bias. Such rectifying characteristic may occur due to creation of a potential barrier in either highly n-doped tin oxide semiconductor and intrinsic n-type titanium oxide interface, or Al/semiconductor interfaces [12]. Because the Schottky barrier (metal–semiconductor contact) must be low due to the similar energies between metal work function and the conduction band of both semiconductors, the higher disorder in the semiconductors interface suggests this region is likely to present the most concentration of potential barriers responsible for the charge carriers trappings, and then, dominate the device transport properties.

A differential negative resistance (DNR) appears for excitation at 54 mW/cm^2, Fig. 4, between 20 and 30 V, which is reduced for excitation at 62 mW/cm^2, and no longer appears at 96 mW/cm^2. The DNR may occur due to electron-trapping at the above mentioned defects within the semiconductors and their interface with Al electrodes. The photoexcitation at power light of 54 mW/cm^2 reaches the limit of the charge ionization at 20 V, when predominant state-defects start to capture electrons. With slightly higher power light of 62 mW/cm^2 similar release of charges is achieved, although the DNR region is reduced. However, at 96 mW/cm^2 the DNR is extinguished probably due to higher release of charges that overcomes the charge trapping effects. The DNR and state-defects may also be related to reduction processes of Sb^{5+} to Sb^{3+} ions, as well as the increased presence of Sb^{3+} segregated at grain boundaries due to high Sb doping in the SnO_2 thin films [32]. Sb^{3+} acceptor ions work as traps for free electrons in the SnO_2 thin film.

The oscillating output current curves at different power lights may occur due to the high voltage operation and to different rates of carrier de-trapping. The high voltage operation presented in our samples may be reduced through the use of interdigitated electrodes, producing a large ratio

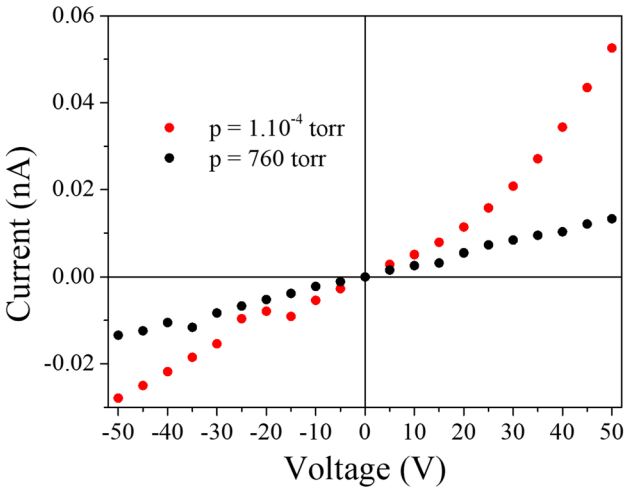

Fig. 5 Current versus Voltage curves for 4 at%Sb:SnO_2/TiO_2 thin films under low pressure, at 10^{-4} torr, and room atmosphere

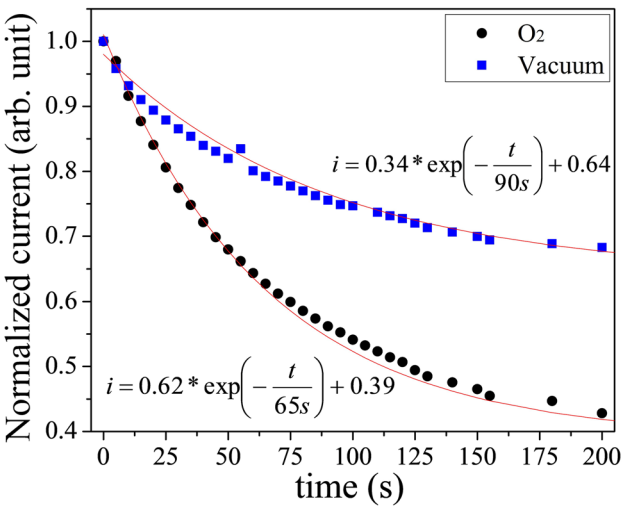

Fig. 6 Normalized decay of photoinduced current under vacuum and O_2 atmosphere at 300 K. Excitation done by InGaN LED for 90 s. Detail: equations used for the exponential fit

between surface exposed area and short contacts distance. Due to the smaller distance between contacts, and new configuration, it could also increase the output electric current.

The same sample characterized by photoexcitation at room atmosphere was investigated concerning its properties as gas sensor. Reduced and room atmosphere pressures were considered in order to investigate the electric response and effects of gas adsorption on superficial defects of the heterojunction. Figure 5 presents the electric response for different atmospheres, which shows the increase in resistance (about 135%) when in air compared with low pressure condition (10^{-4} torr). This reduced electrical current in air atmosphere is related to trapping of free electrons due to the adsorbed oxygen ionic species from the air composition on the semiconductors' surface, thus, reducing the free charge carrier and electrical current [33, 34].

3.3 O_2 gas influence on decay of photoinduced current

The gas sensing properties of the TiO_2 thin film is better investigated and evaluated concerning its enhancement under monochromatic light excitation, with energy below the TiO_2 bandgap. Figure 6 shows experimental decay of photo-induced conductivity under vacuum and O_2 atmospheres (1 atm). A simple theoretical analysis of this decay is done in order to potentially enhance the efficiency of gas sensing properties of this material and the lateral junction with Sb:SnO_2. Data shown in Fig. 6 refers to experimental decay of photo induced current under vacuum and O_2 atmospheres (1 atm). In this sort of experiment, the TiO_2 anatase sample, with Al electrodes as shown in Fig. 1b, is irradiated with light (InGaN LED) for a fixed time of 90 s, until the current practically reaches saturation. Then the illumination source is removed and the current decay is recorded under a constant applied voltage V = 2V.

In Fig. 6, the recorded current data is normalized by the maximum current (time zero), in order to show the differences in the electron trapping behavior. It is important to mention that the excitation source has energy below the TiO_2 bandgap, which assures no electron–hole pair generation. Therefore, this characterization aims the investigation of intra bandgap energy defects that are ionized by light irradiation under different atmospheres. The current as function of time *i(t)* after removing the illumination can be given by:

$$i(t) = K_\sigma \times q \times n(t) \times \mu \quad (1)$$

where K_σ is the constant between current and conductivity, q is the elementary charge, $n(t)$ is the time-dependent free electron concentration, and μ is the carrier mobility that is assumed to be dominated by grain boundary scattering [35], and therefore, varies only with the temperature for the same material, being constant in the present case where the decay is measured at room temperature. The electron concentration (n) after the illumination is removed is given by [36]:

$$\frac{dn}{dt} = -C_n \times N_{Def} \quad (2)$$

where C_n is the capture rate given by $V_{th} \times \sigma_n \times n$, where V_{th} is the thermal velocity, σ_n is the electron capture cross section, $\sigma_n = \sigma_\infty \times exp(-E_{cap}/kT)$, σ_∞ is the high temperature capture cross section and E_{cap} is the capture barrier. Considering that N_{Def}, the ionized defect concentration, in this sol–gel material is practically constant due to highly disordered structure, the solution of Eq. (2) is given by:

$$n = -n(0) \times \exp(-C_1 \times t) \quad (3)$$

where $n(0)$ is the initial electron concentration at t = 0, when the illumination has just been removed, and C_1 is given by $V_{th} \times \sigma_\infty \times N_{Def} \times exp(-E_{cap}/kT)$.

A complete analysis of the transient decay of the photo-induced current has been done for AlGaAs [36] and SnO_2 [37, 38], and, in order to get quantitative parameters, the decay must be performed at several temperatures. However, the present analysis is done only at room temperature and intends to obtain qualitative data, in order to compare decay data obtained under different atmosphere conditions. A similar approach, for data generated only at room temperature, has been presented recently for Eu-doped SnO_2 [39].

A simple exponential fit of the experimental equation yields the Eq. (4):

$$i = A_1 \times \exp\left(-\frac{t}{k_1}\right) + A_2 \tag{4}$$

where the fitting parameters A_1, A_2, and k_1 are summarized in details in Fig. 6. The term A_2 implies that there is a steady state-like current, which actually decays with very long time constant. Then, this term can be replaced by another exponential in Eq. (4), where the decay regime is for much longer time (not shown in Fig. 6), which means that the trapping is done by other sort of defect. Therefore, for a more complete exponential fit the measurement should be done for longer time, and Eq. (4) should be replaced by two exponentials, with trapping rate characteristics of each defect [39]. However, in order to interpret the decay rates by defects immediately affected by the distinct atmospheres, we may compare only the time constant of the Eqs. (1, 4) to obtain that:

$$V_{th} \times \sigma_\infty \times N_{Def} \times \exp\left(-\frac{E_{cap}}{kT}\right) = {k_1}^{-1} \tag{5}$$

Then, applying the Eq. (5) for both decays under vacuum and O_2 atmospheres, and dividing the first by the second, one obtain:

$$E_{cap}(O_2) - E_{cap}(vacuum) = kT \ln\left(\frac{k_1[O_2]}{k_1[vacuum]}\right) \tag{6}$$

It is important to mention that E_{cap}, the capture barrier, is the potential to be overcome by the electrons to get trapped back at the defects. It is related to lattice relaxation to transform the ionized defect to a neutral state. The parameters k_1 obtained from the exponential fitting of experimental data shown in Fig. 6, obtained for vacuum and O_2 atmospheres, yields an energy difference between the capture energies of about 10 meV. Although this difference is rather small to explain the significant difference in the decay behavior of both cases, it is enough to affirm that the trapping is dominated by distinct defects in each case. Considering the undoped nature of the TiO_2 sample, we believe that the trapping is done by oxygen vacancies in the vacuum case, and adsorbed oxygen species in the O_2 atmosphere case. The obtained result means that the lattice relaxation is higher for the dominant defect in vacuum (oxygen vacancies) compared to the electron trapping by adsorbed oxygen species, which explains the slower decay in vacuum when compared to oxygen-rich atmosphere.

This result emphasizes the interest in TiO_2 samples for gas adsorption sensors and show that the adequate use of light may improve the current sensibility and moreover, may help to select the preferential defect trapping. The combination of TiO_2 with SnO_2 may improve even further this property. Floriano and coworkers [40] suggested the use of TiO_2 as exposed (top) layer due to higher electronic affinity of TiO_2. Our suggestion is the use of light concomitant with the gas adsorption in order to increase the sensing efficiency in the gas detection route, as shown in photocurrent decay of Fig. 6.

4 Conclusions

In summary we have presented the gas and photo sensing properties of the $Sb:SnO_2$ and TiO_2 thin films deposited by sol–gel dip-coating. The photosensitivity of these films in a lateral junction was investigated with different powers of solar light spectra, and it was found to be caused by defects within the semiconductors, their interface, and metal/semiconductors interface. The same films were evaluated on different atmosphere pressures, and a higher conductivity at lower pressure was found, which we relate to reduction on surface adsorption of oxygen ionic species. TiO_2 film based devices were also investigated concerning the gas-sensitivity under photexcitation in vacuum and O_2 atmospheres. It was presented that the decay of photo-induced current under oxygen-rich atmosphere is faster compared to results obtained under vacuum atmosphere. The capture energy was qualitatively evaluated and has shown a significant higher barrier energy for experimental results under vacuum, which implies the charge trapping by adsorbed oxygen species under O_2 atmosphere occurs more frequently than other defects within the TiO_2 thin film. These results show the functionality of the TiO_2 and $Sb:SnO_2$ deposited by sol–gel may be improved for gas-sensitivity by using light along the detection.

Acknowledgements We acknowledge Ana H. C. Maciel for her participation in the current–voltage under solar light spectra photo-excitation, Prof. Dr P.N. Lisboa and MSc L.D. Trino for help with TiO_2 solution processing. We also would like to thank Prof. Dr C.F.O. Graeff and L.G.S. Albano for solar light simulator and electrical measurement-software interface. This work was financially supported by CAPES, FAPESP (2017/10766-1), AUXE/PROEX (2330/2015), and CNPq (305963/2016-3).

References

1. O. Carp, C.L. Huisman, A. Reller, Prog. Solid State Chem. **32**, 33 (2004)
2. W. Zeng, T. Liu, Z. Wang, Sensors Actuators B **166–167**, 141 (2012)
3. J. Nisar, Z. Topalian, A. De Sarkar, L. Osterlund, R. Ahuja, ACS Appl. Mater. Interfaces **5**, 8516 (2013)
4. M.H. Boratto, L.V.A. Scalvi, J.L.B. Maciel Jr., M.J. Saeki, E.A. Floriano, Mater. Res. **17**, 1420 (2014)
5. G. Sanon, R. Rup, A. Mansingh, Phys. Rev. B **44**, 5672 (1991)
6. V. Geraldo, L.V.A. Scalvi, P.N. Lisboa-Filho, C. Morilla-Santos, J. Phys. Chem. Solids **67**, 1410 (2006)
7. E.A. Floriano, L.V.A. Scalvi, J.R. Sambrano, A. De Andrade, Appl. Surf. Sci. **267**, 164 (2013)
8. V. Skoromets, H. Němec, J. Kopeček, P. Kužel, K. Peters, D. Fattakhova-Rohlfing, A. Vetushka, M. Müller, K. Ganzerová, A. Fejfar, J. Phys. Chem. C **119**, 19485 (2015)
9. A.G. Milnes, D.L. Feucht, *Heterojunctions and Metal-Semiconductor Junctions*. (Academic Press, New York, 1972)
10. L.P. Ravaro, L.V.A. Scalvi, M.H. Boratto, Appl. Phys. A **118**, 1419 (2014)
11. R.A. Ramos Jr., M.H. Boratto, M.S. Li, L.V.A. Scalvi, Mater. Res. **20**, 866 (2017)
12. M.H. Boratto, R.A. Ramos Jr., M. Congiu, C.F.O. Graeff, L.V.A. Scalvi, Appl. Surf. Sci. **410**, 278 (2017)
13. D.O. Scanlon, C.W. Dunnill, J. Buckeridge, S.A. Shevlin, A.J. Logsdail, S.M. Woodley, C. Richard, A. Catlow, M.J. Powell, R.G. Palgrave, I.P. Parkin, G.W. Watson, T.W. Keal, P. Sherwood, A. Walsh, A.A. Sokol, Nat. Mater. **12**, 798 (2013)
14. W.G. Oldham, A.G. Milnes, Solid. State. Electron **6**, 121 (1963)
15. I. Kim, W.Y. Choi, Int. J. Nanotechnol. **14**, 155 (2017)
16. M. Kunst, T. Moehl, F. Wünsch, H. Tributsch, Superlattices Microstruct. **39**, 376 (2006)
17. Y. Cao, X. Zhang, W. Yang, H. Du, Y. Bai, T. Li, J. Yao, Chem. Mater. **12**, 3445 (2000)
18. B. Levy, W. Liu, S.E. Gilbert, J. Phys. Chem. B **101**, 1810 (1997)
19. R.E. Presley, C.L. Munsee, C.-H. Park, D. Hong, J.F. Wager, D.a Keszler, J. Phys. D. Appl. Phys. **37**, 2810 (2004)
20. B.J. Choi, D.S. Jeong, S.K. Kim, C. Rohde, S. Choi, J.H. Oh, H.J. Kim, C.S. Hwang, K. Szot, R. Waser, B. Reichenberg, S. Tiedke, J. Appl. Phys. **98**, 33715 (2005)
21. D. Guo, A. Ito, T. Goto, R. Tu, C. Wang, Q. Shen, L. Zhang, J. Adv. Ceram. **2**, 162 (2013)
22. M. Okuya, K. Nakade, S. Kaneko, Sol. Energy Mater. Sol. Cells **70**, 425 (2002)
23. G. Oskam, A. Nellore, R.L. Penn, P.C. Searson, J. Phys. Chem. B **107**, 1734 (2003)
24. L.D. Trino, Desenvolvimento e Otimização de Materiais Nanocristalinos Para Células Solares Sensibilizadas, UNESP (2014)
25. M.H. Boratto, L.V.A. Scalvi, L.V. Goncharova, G. Fanchini, J. Am. Ceram. Soc. **99**, 4000 (2016)
26. N. Ghobadi, Int. Nano Lett. **3**, 2 (2013)
27. M. Dou, C. Persson, J. Appl. Phys. **113**, 83703 (2013)
28. S. Cardoso, C. Longo, M. De Paoli, Quim. Nov. **28**, 345 (2005)
29. N. Sommer, J. Hupkes, U. Rau, Phys. Rev. Appl. **5**, 24009 (2016)
30. C. Terrier, J.P. Chatelon, J.A. Roger, Thin Solid Films **295**, 95 (1997)
31. G. Mor, K. Shankar, M. Paulose, O.K. Varghese, C.A. Grimes, Nano Lett. **6**, 215 (2006)
32. V. Geraldo, V. Briois, L.V.A. Scalvi, C.V. Santilli, J. Phys. Chem. C **114**, 19206 (2010)
33. J. Watson, K. Ihokura, G.S.V Coles, Meas. Sci. Technol **4**, 711 (1993)
34. W. Göpel, G. Rocker, R. Feierabend, Phys. Rev. B **28**, 3427 (1983)
35. D.H. Zhang, H.L. Ma, Appl. Phys. A Mater. Sci. Process **62**, 487 (1996)
36. T.W. Dobson, L.V.A. Scalvi, J.F. Wager, J. Appl. Phys. **68**, 601 (1990)
37. E.A. Morais, L.V.A. Scalvi, J. Mater. Sci. **42**, 2216 (2007)
38. E.A. Morais, L.V.A. Scalvi, A.A. Cavalheiro, A. Tabata, J.B.B. Oliveira, J. Non. Cryst. Solids **354**, 4840 (2008)
39. C.F. Bueno, L.V.A. Scalvi, Thin Solid Films **612**, 303 (2016)
40. E.A. Floriano, L.V.A. Scalvi, M.J. Saeki, J.R. Sambrano, Phys. Chem. A **118**, 5857 (2014)